Cement and Concrete Composites 92 (2018) 145–154

Contents lists available at ScienceDirect

Cement and Concrete Composites

journal homepage: www.elsevier.com/locate/cemconcomp

Dispersion of graphene oxide agglomerates in cement paste and its effects on electrical resistivity and flexural strength

Xiangyu Li[a,*], Linhao Wang[a], Yuqing Liu[b], Wengui Li[c], Biqin Dong[b], Wen Hui Duan[d]

[a] College of Architecture and Civil Engineering, Taiyuan University of Technology, Shanxi, 030024, China
[b] Department of Civil Engineering, Guangdong Provincial Key Laboratory of Durability for Marine Civil Engineering, Shenzhen University, Shenzhen, 518060, China
[c] Center for Built Infrastructure Research, School of Civil and Environmental Engineering, University of Technology Sydney, NSW, 2007, Australia
[d] Department of Civil Engineering, Monash University, Melbourne, VIC, 3800, Australia

ARTICLE INFO

Keywords:
Graphene oxide
Dispersion
Cement
Electrical resistivity

ABSTRACT

Actual dispersion of graphene oxide (GO) in cement paste was investigated by using both X-ray computed tomography and X-ray photoelectron spectroscopy. It was found that GO nanosheets are mainly agglomerated, as an individual phase, with platelet-like morphology and little GO being absorbed onto surfaces of cement particles and hydration products. By performing an electrical resistivity test, GO agglomerates are found to be more electrically insulative than cement paste. Therefore, it is not possible to develop self-sensing cement composites by incorporating GO directly without resolving its dispersion issue. However, GO agglomerates enhance the flexural strength of cement paste because of their special morphology and intrinsic strength. Results showed that the flexural strength of cement paste was increased by 83% with incorporation of 0.04% GO by weight of cement.

1. Introduction

Graphene oxide (GO) is a two-dimensional nanomaterial derived from graphite by inserting several oxygen functionalities into the parent graphene backbone [1]. GO's superior mechanical properties, high dispersibility in water, and low production cost make it a promising reinforcing material for enhancing the properties of cementitious composites [2–5]. By conducting reactive molecular dynamics simulation, Hou et al. [6] investigated the intrinsic interactions between a GO nanosheet with cement hydration products. It was reported that, if GO could be dispersed in nanosheets form in a cementitious matrix, compared to graphene, GO incorporation endows the cement composite with a higher cohesive force and enhanced plasticity owing to the H-bonds and covalent–ionic bonds. However, it was conjectured that, when the GO nanosheets are introduced into the cementitious matrix, significant agglomerations would occur as the result of chemical cross-linking [7] by the calcium cations that are abundant in cement pore solutions. As reported in prior studies [8–10], GO agglomerates were observed in synthetic pore solutions or cement paste under unusually high GO dosage (0.4% and 0.8% by weight of cement). Under normal dosage of GO (0.02% and 0.04% by weight of cement), direct observation of the actual dispersion of GO agglomerates in cement paste has not been successful owing to the low content and poor contrast between GO and cement hydrates under scanning electron microscopy (SEM). Therefore, the actual dispersion of GO under normal dosage in cement paste remains unclear.

From a dispersion perspective, GO incorporated into cement paste can be divided into two types: absorbed GO and individual GO. When GO nanosheets are introduced into cement composites, they may be absorbed onto surfaces of reacting cement particles and hydration products by the electrostatic attractive force. They also could exist as individual GO in the form of agglomerates or nanosheets. Individual GO could, theoretically, take the form of agglomerates or a single nanosheet. However, based on prior studies, single-sheet GO cannot exist in cement composites because of the chemical cross-linking of calcium cations [11,12]. Compared to observing GO dispersion by SEM, X-ray computed tomography (CT) is a nondestructive technique for visualizing features in the interior of opaque solid objects. In addition, relatively large three-dimensional (3D) samples can be used in CT to obtain a complete view of GO dispersion in cement composites by observing a large number of two-dimensional (2D) images, whereas, with SEM, only a very small area can be observed at one time. By using CT, dispersion of carbon fiber was quantitatively analyzed based on cross-sectional images of successive layers in cement composites [13,14]. The CT technique was also used to study the microstructure of nanoparticle-incorporated cement paste. The pore structure of cement paste

* Corresponding author.
E-mail address: lixiangyu@tyut.edu.cn (X. Li).

https://doi.org/10.1016/j.cemconcomp.2018.06.008
Received 6 February 2018; Received in revised form 9 May 2018; Accepted 11 June 2018
Available online 19 June 2018
0958-9465/ © 2018 Elsevier Ltd. All rights reserved.

incorporated with reduced GO (rGO) was investigated using 3D CT [15]. However, in Ref. [15], the resolution of 100 μm was not high enough to capture rGO dispersion information, except for pores and air voids. It should be noted that, with the CT technique, it is only possible to observe individual GO owing to resolution limitation (normally on the order of a micrometer). Moreover, X-ray photoelectron spectroscopy (XPS) might be helpful in detecting any GO nanosheet absorbed onto surfaces of hydration products or cement particles. Wang et al. [16] reported adsorption characteristics of GO nanosheets on cement particles. However, in Ref. [16], they added small amount of cement (0.09 g) into a GO solution (60 g) to study GO adsorption onto cement particles. The water to cement ratio was ~667 (60/0.09), which is much larger than usually adopted values (of < 1). Therefore, their adsorption characteristics might not reflect the actual case in cement paste incorporated with GO for normal water to cement ratio and GO dosage. Based on the above introduction and prior studies, it is viable to investigate the actual dispersion of GO in cement paste by conducting CT and XPS analysis to study individual GO agglomerates and absorbed GO, respectively.

In this study, we used the X-ray micro CT (X-ray μCT) technique with resolution extended to 1 μm to investigate the actual dispersion of GO agglomerates in cement paste. XPS analysis was conducted to investigate GO absorbed onto surfaces of hydration products or cement particles. In addition, GO agglomerates in cement paste were also observed by SEM on cement paste samples after ion polishing. Then, the effects of GO agglomerates on the electrical resistivity and flexural strength of the cement paste were investigated.

2. Materials and sample preparation

2.1. GO

Aqueous GO suspensions with concentration of 4 mg/ml were produced by Graphenea® (Spain). In the as-received GO suspension, no surfactant was used to stably disperse the GO owing to its hydrophilicity. Elemental analysis of GO showed a carbon to oxygen ratio of ~1.1, suggesting a relatively high oxidation degree. The hydrodynamic size of GO nanosheets was measured by using a dynamic laser scattering method following a well-established procedure [17]. GO sizes were Gaussian distributed and the mean diameter of GO nanosheets was ~847.3 nm.

2.2. Cement powder

General purpose ordinary Portland cement (OPC) conforming to ASTM C150 was used throughout the study. The chemical composition measured by X-ray fluorescence (XRF) of the cement is listed in Table 1.

2.3. Preparations of cement paste samples

Cement paste samples were fabricated by using a high-speed shear mixer (CTE Model 7000). The mixing procedure similar to that in ASTM C1738-11a was adopted. Before mixing with cement powder, the correct amount of diluted GO solution was ultrasonicated for 5 min for improving the dispersion of GO nanosheets. Then, the solution was placed in the mixing bowl and mixing was started at 4000 rpm while the correct amount of cement powder was added to the GO solution over a 30 s period. Mixing was continued at 4000 rpm for another 30 s then switched to 12000 rpm for another 30 s of mixing. The mixer was then switched off and the mixture was left to stand for 150 s before any material collected on the side of the bowl was scraped down. Final mixing for 30 s was done at 12000 rpm.

Table 1
Composition of cement powder.

Oxide	Al_2O_3	SiO_2	CaO	Fe_2O_3	K_2O	MgO	Na_2O	SO_3	LOI
%	4.7	19.9	63.9	3.4	0.5	1.3	0.2	2.6	3.0

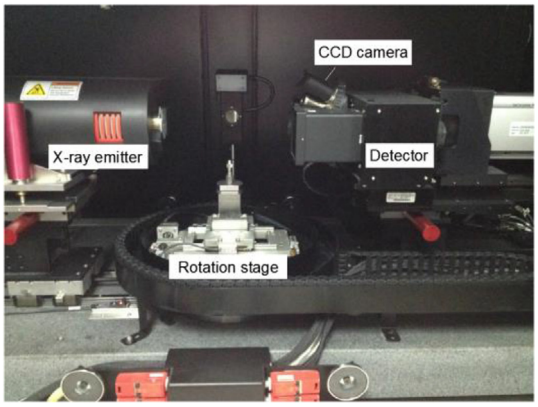

Fig. 1. Internal features of XRadia Micro XCT-400.

The water to cement ratio for all cement paste samples was fixed at 0.4. According to different GO dosage, the samples were denoted as CGn, in which n refers to GO dosage. Four different GO dosages were applied in this study, 0.01%, 0.02%, 0.03%, and 0.04% by weight of cement. For example, CG4 refers to cement paste samples containing 0.04% GO by weight of cement. The reference sample without adding GO was denoted as C.

3. Experiments

3.1. X-ray μCT

Dispersion of GO agglomerates in cement paste were investigated by using an X-ray μCT system (XRadia Micro XCT-400) located at Shenzhen University (China). As shown in Fig. 1, the X-ray μCT system comprised a micro-focus X-ray emitter, a rotation stage that allows for 360° imaging, an image intensifier detector with three multiple charge-coupled device (CCD) cameras, and an image processing unit. The X-ray tube used in this study was equipped with a small focal spot (micro-focus X-ray-tube) and optical magnification enabled a high resolution. By means of X-ray μCT, the resolution of volumetric picture elements (voxels) was extended to 1 μm. In addition, the working distances between source, sample, and detector were typically ~100 mm in this system, which means full tomography can be achieved even for larger samples.

Cement paste samples C and CG4 were investigated by using X-ray μCT to study dispersion of GO agglomerates in CG4. Cylindrical C and CG4 samples were prepared by pouring a fresh C and CG4 mixture into a plastic tube with an inner diameter of 5 mm. Then the samples were vibrated to ensure good compaction. The samples were observed by X-ray μCT after curing for 7 days at a temperature of 20 °C and a relative humidity of 95%.

In this study, a 1024 × 1024 pixel X-ray camera was used while considering four elemental parameters. The applied X-ray source excitation was 80 keV and the current was 101 μA, as selected according to sample geometry and material compositions, while the magnification was 4×. The reconstructed image matrix has a volume of 1024 × 1024 × 1000, corresponding to 1000 slices of 1024 × 1024 pixels each, while respective pixel size and voxel size were 4.5413 μm and 4.5413 × 4.5413 × 4.5413 μm^3, respectively. The X-ray absorption of each voxel, represented by the material-specific X-ray absorption coefficient, was normalized to 8-bit gray values.

3.2. XPS

XPS measurements were performed on an ESCALAB 250Xi photoelectron spectrometer (Thermo Fisher) by using a monochromatic Al Kα X-ray source as incident radiation. XPS spectra were recorded in the fixed transmission mode. The analyzer slit width was set to 900 μm and a pass energy of 200 eV was chosen. The binding energies were calibrated based on the graphite C1s sp3 peak at 284.8 eV [18]. Before measurement, cylindrical samples C and CG4 were grinded to have one end smooth to improve the quality of results. The Avantage v5.979 XPS program with a Gaussian–Lorentzian mix function (L/G = 30%) and smart (modified Shirley) background subtraction was employed to deconvolute the XPS spectra. The full width at half maximum (FWHM) values were fixed at a maximum limit of 3.5 eV for all of the peaks during the fitting procedure. The peak positions were reproducible along with the fixed Lorentz to Gaussian ratio and FWHM. Care was taken to ensure that all the fitting results were self-consistent, so that the corresponding deconvoluted peaks could be compared quantitatively.

3.3. SEM

The microstructure of cement paste incorporated with GO was studied by using SEM. The sample prepared for SEM was first grinded then polished by using a cross-section ion polisher (IB-09010 C < superscript > < /superscript > P, JEOL). A thin layer of gold–palladium was then deposited onto the polished surface of the samples. Energy-dispersive X-ray spectroscopy (EDS) spectra analysis was conducted on the surface of the samples to study their elemental distributions.

3.4. Electrical resistivity measurements of GO-incorporated cement pastes

In this study, a two-pole method was employed for obtaining the electrical resistivity of the GO-incorporated cement paste specimens, namely C, CG1, CG2, and CG4, with two electrodes being used.

The cement paste samples were first prepared and then cured for 28 days at a temperature of 20 °C and a relative humidity of 95%. After curing, the specimens were put into an oven operating at 60 °C for 3 days followed by 95 °C for another 3 days, for eliminating the polarization effect during electrical resistivity measurements [19]. The exterior dimensions of the specimens used for electrical resistivity measurement were 110 mm × 15 mm × 15 mm. Copper tape of 10 mm in width, to serve as electrodes for electrical resistivity measurements, were glued by using silver conductive paste around the whole perimeter at both ends perpendicular to the length of the specimens.

A concrete resistivity meter (Giatec RCON™) was used to measure impedance between the two copper tape electrodes glued on the specimens. The test setup is shown in Fig. 2. An AC current was applied across the two copper tape electrodes. The frequency of 1000 Hz was adopted because it is relatively low and can minimize the polarization effects of cement-based materials [20]. The stimulus time of each frequency was ~5 s. The voltage produced across the same electrodes was then measured. Impedance across the copper tape electrodes was calculated by the resistivity meter as a complex ratio of voltage and current. The phase angle (θ) of the measured impedance was also recorded. Therefore, the bulk resistivity can be calculated by using

$$\rho = \frac{RA}{L}\cos(\theta), \tag{1}$$

where R is the measured impedance, A is the cross-sectional area of the specimen (15 mm × 15 mm), and L is the distance between the two copper electrodes (100 mm). The environmental conditions, temperature and humidity, significantly influence resistivity, but these were kept constant throughout all experiments in this study.

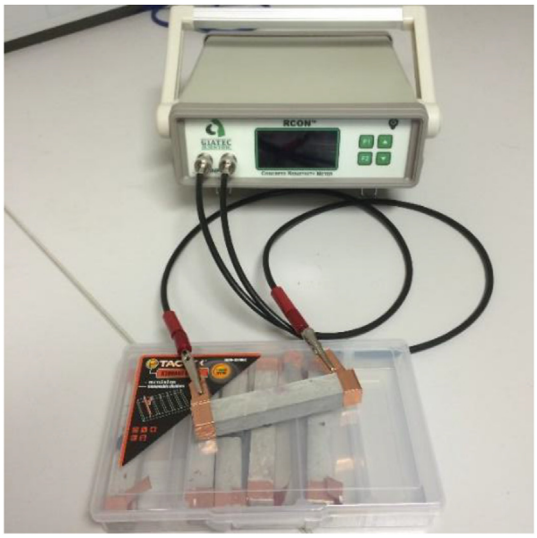

Fig. 2. Resistivity test setup.

3.5. Flexural strength test of GO-incorporated cement pastes

The flexural strength of GO-incorporated cement paste was determined by using a three-point bending setup subjected to a point load by an Instron testing machine according to ASTM C78/C78M-10. The loading rate was 0.02 mm/min. The dimensions of the specimens for flexural testing were 75 mm × 15 mm × 15 mm. Before testing, the specimens were cured for 28 days at a temperature of 20 °C and a relative humidity of 95%.

4. Results and discussion

4.1. Dispersion of GO agglomerates observed by using X-ray μCT

X-ray μCT was used to measure the attenuations of a specimen being excited by a polychromatic beam of X-ray photons with an appropriate detector. As X-ray photons are absorbed and scattered by the specimen, the incident intensity is attenuated and the transmitted intensity is then recorded by the detector. The attenuation behavior of X-ray photons can be described by the Beer–Lambert law

$$I = I_0(x)\cdot e^{-\int_0^x u(\rho,Z,E)dx}, \tag{2}$$

where I is the transmitted intensity, I_o is the incident intensity, u *is* the linear attenuation coefficient as dependent on density ρ, atomic number Z, and energy E, and x is the specimen thickness. CT images were created based on intensity measurements at different angles. The images can be used to distinguish structural and material characteristics according to variations of intensity. According to Eq. (2), the intensity measurement at a certain spot within the specimen is dependent on the density and atomic number of the material composing the spot. In addition, the CT intensity value is quantified on a 0–255 grayscale to provide a high-quality display. Substances with higher density exhibit higher gray value, which is brighter, while substances with lower density exhibit lower gray value, which is darker.

As shown in Fig. 3, sample C has a few circular pores with the lowest gray value. In addition to circular pores, CG4 has quite a number of slender platelet-like substances with lower density, which should be GO agglomerates. Previous study [10] showed that GO agglomerates have ellipse-like shape with mean length (the longest dimension of GO agglomerates) of 45.9 μm, which is much larger than the width (dimension perpendicular to the longest dimension). The thickness of GO agglomerates are below than 10 nm since they are mainly multi-layer (4–10 layers) GO on the basis of UV-vis analysis [8]. Accordingly, GO

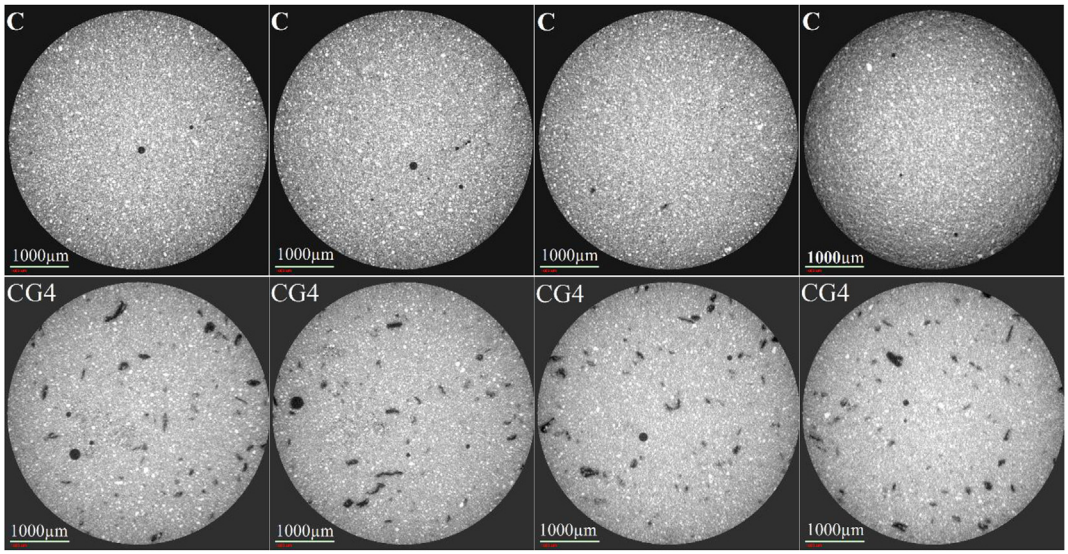

Fig. 3. 2D sliced images of C (top) and CG4 (bottom) obtained by using X-ray μCT.

agglomerates still have 2D platelet-like morphology with both length and width are much larger than thickness. Based on above discussions, CT observations of GO agglomerates is in line with previous study. These slender platelet-like substances were not observed in Ref. [15], which might be due to their lower resolution (100 μm) and different dispersion condition of reduced GO. Although it is difficult to obtain an accurate size distribution of these platelet-like GO agglomerates, one can observe that some of them are around hundreds of micrometers, which is much larger than the original nanosheet size. It was also shown that the GO agglomerates were dispersed randomly and uniformly within the cement matrix. Density of GO agglomerates can be estimated by appropriately scaling [21] the density of fully dense graphite (2.25 g/cm^3) with interlayer spacing of 0.34 nm. The density of dry GO agglomerates was estimated as 0.70 g/cm^3 with interlayer spacing of 1.09 nm [7]. Then, the density of GO agglomerates with water content can be estimated as ~1.70 g/cm^3, which is consistent with molecular dynamics calculations [22]. Therefore, sample C is a two-phase composite with pores and cementitious solid matrix. CG4 is a three-phase composite with pores, GO agglomerates, and cementitious solid matrix. Fig. 4 shows 3D CT images of C and CG4. It was also shown that GO agglomerates dispersed randomly and uniformly within the whole matrix.

Fig. 5a shows the gray value distributions for CT images of C and CG4. As mentioned above, unhydrated cement particles have the highest density and present the highest gray values. As shown in Fig. 5, compared to C, CG4 has a smaller amount of unhydrated cement particles, which indicates the hydration acceleration effect of GO addition. This is consistent with research findings in a previous study [9]. Fig. 5b and c show differential gray value distributions for C and CG4. As shown in Fig. 5b and c, there are two peaks observed in the distribution of sample C without GO addition; these stand for two different components, pores and solid matrix. The pores have the lowest density and therefore the lowest gray values, from 0 to ~50. The solid matrix of the cement paste includes hydration products and unhydrated parts, while the latter has the highest density. Therefore, compared to pores, the solid matrix has a higher density and higher gray values, from ~50 to 255. Fig. 5c shows that, for CG4, there are three peaks, which stand for the three different components in GO-incorporated cement paste. The gray values from 0 to ~50 are for pores, which have the lowest density, the gray values from ~50 to ~100 indicate the GO agglomerates, which have medium density, and the gray values > 100 reveal the cementitious solid matrix with the highest density. In the literature, dispersion of carbon fibers was also studied by using X-ray CT technology. It was reported that pores, carbon-fiber bundles, and carbon-fiber-free areas can be identified by gray value distribution [14], following an increase of gray value from pores with the lowest density to carbon-fiber bundles with medium density to carbon-fiber-free areas (cementitious solid matrix) with the highest density. This is consistent with the results of the current study.

4.2. SEM

Fig. 6 shows SEM images of GO agglomerates. In Fig. 6a, one can observe a GO agglomerate with a lateral dimension of ~304 μm. Compared with GO agglomerates with wrinkled and folded morphology found in a previous study [8], the morphology of GO agglomerates observed in the current study was different. However, it is reasonable to assume that the smooth surface of the GO agglomerate was produced by the ion polishing process. Interfacial zones between GO agglomerates and the cement matrix are shown in Fig. 6b and d at different magnifications. In general, the interfacial zones were found to be dense and compact. In addition, the transition from GO agglomerate to cement matrix was smooth, indicating good bonding between them. However, future work is needed to investigate the mechanical bonding between GO agglomerates and the cement matrix by nanoindentation. In addition to morphological observations, elemental analysis of GO agglomerates was conducted by using EDS to scan an area containing one GO agglomerate. As shown in Fig. 7, the GO agglomerate contained a large amount of carbon and oxygen, while a certain amount of calcium element was also found in the agglomerate. According to mechanism described in a previous study [8], the calcium content found in GO agglomerates is responsible for chemical cross-linking of individual GO nanosheets.

4.3. XPS study of C and CG4

Fig. 8 depicts Ca2p and Si2p XPS spectra of cement paste with and without GO incorporation. It is shown that the photoelectron intensities for both Ca and Si remain unchanged after GO incorporation with GO dosage of 0.04% by weight of cement. Given the detection accuracy of XPS, this indicates that there is little GO absorbed onto surfaces of cement particles and hydration products. The result is consistent with what was reported in a previous study [9]. In that prior study, by conducting an isothermal calorimetry test at an early age, it was conjectured that little GO was absorbed onto the surfaces of cement particles or hydration products [9].

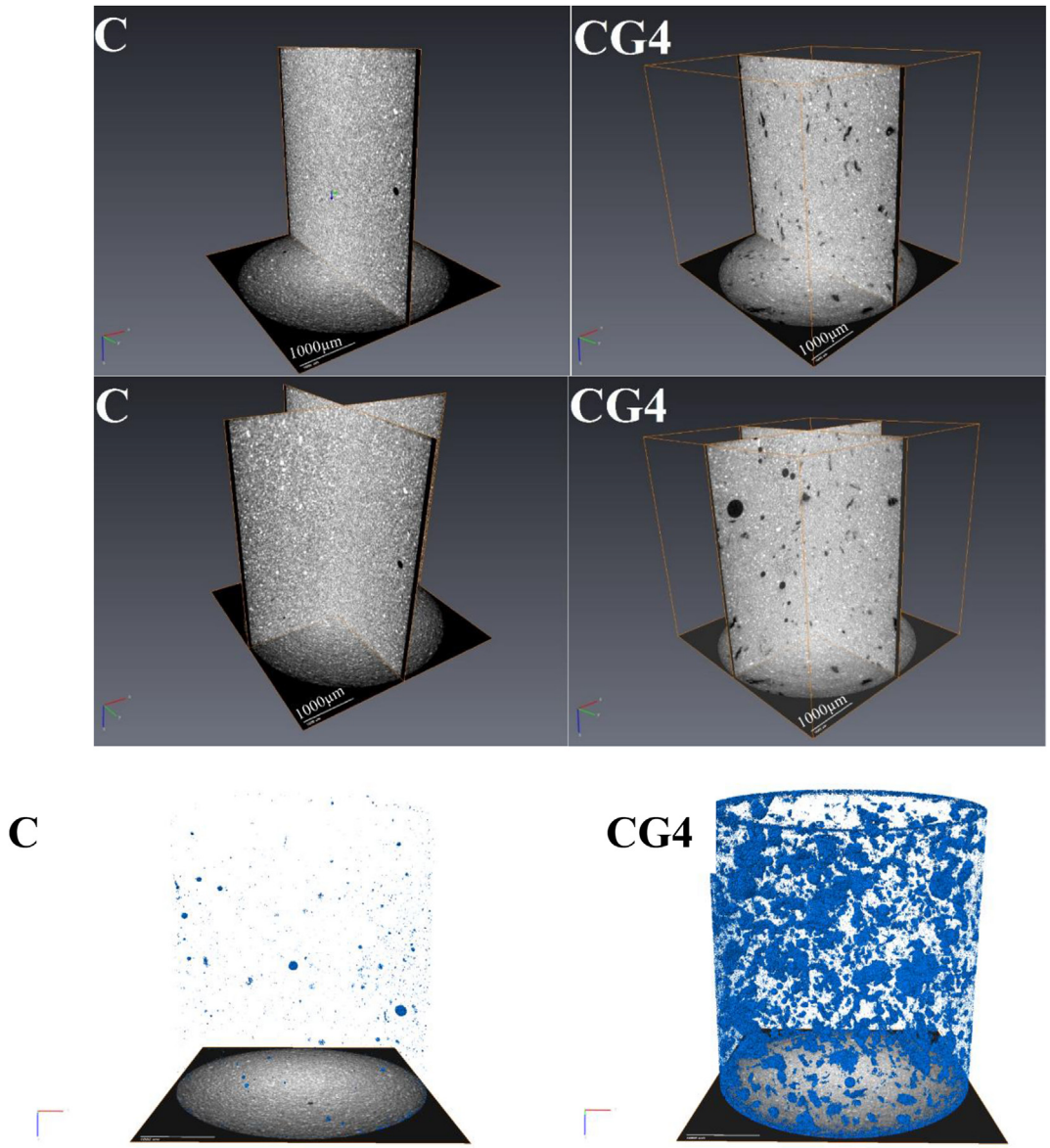

Fig. 4. 3D X-ray CT images of C (left) and CG4 (right) samples.

Adsorption of GO onto surfaces of hydrating cement particles can be understood by the competition between adhesive energy and mechanical deformation [23]. According to DLVO theory, the adhesive energy between GO nanosheets and hydrating cement particles comes from electrostatic and van der Waals attractions. For hydrating cement particles, a heterogeneous charge distribution is developed on its surface owing to various clinker phases and hydration products [24]. Therefore, if adsorption occurs, GO nanosheets would be attracted and adsorbed favorably onto positively charged surfaces, including C_3A, C_4AF, and ettringite. However, full contact between GO nanosheets and reacting cement particles has to be achieved for GO nanosheets to be stably adsorbed. To achieve full contact, GO nanosheets have to be mechanically deformed to adapt to surfaces of hydrating cement particles. This would be not easy given the surface roughness of cement particles. Most importantly, the electrostatic attraction is concentrated at the edge of GO nanosheets because carboxyl groups are located along the edges [25]. Given the large surface area of GO, the electrostatic attraction per area could be even weaker. Therefore, it is reasonable to assume that the attraction between GO and hydrating cement particles is too weak to compensate for the mechanical deformation to achieve stable adsorption. In addition, it is not probable for GO agglomerates formed by calcium cross-linking to be adsorbed onto any surface because of its greater stiffness.

The XPS results in the current study differ from what was reported in Ref. [16]. It was reported that Si2p and Ca2p photoelectron intensities of the cement decreased by varying degrees after adsorption of GO nanosheets [16], owing to the large amount of GO being adsorbed onto surfaces of cement particles and hydration products. However, it should be noted that, in Ref. [16], GO dispersion was studied by adding a very small amount of cement to the GO solution. The GO dosage was at least 17% by weight of cement, which is much higher than the 0.04% in the current study. Therefore, in the study of Reference [16], GO was overdosed. It is reasonable to assume that GO content was higher enough to cover complete surfaces of cement particles and hydration products, because the surface area of GO ($5.64\,m^2 = 250\,mg/L \times 60\,ml \times 376.53\,m^2/g$) was much greater than that of cement ($0.03\,m^2 = 0.09\,g \times 3550\,cm^2/g$). In Ref. [16], the thickness of GO adsorbed onto the surface of cement was determined to be 10.16 nm, which means ~10 layers of GO nanosheets (with the thickness of a single GO nanosheet being 0.83 nm) were stacked together. The thickness result of Reference [16] is consistent with what was reported in Ref. [8], in which GO agglomerates were mainly multilayer (4–10

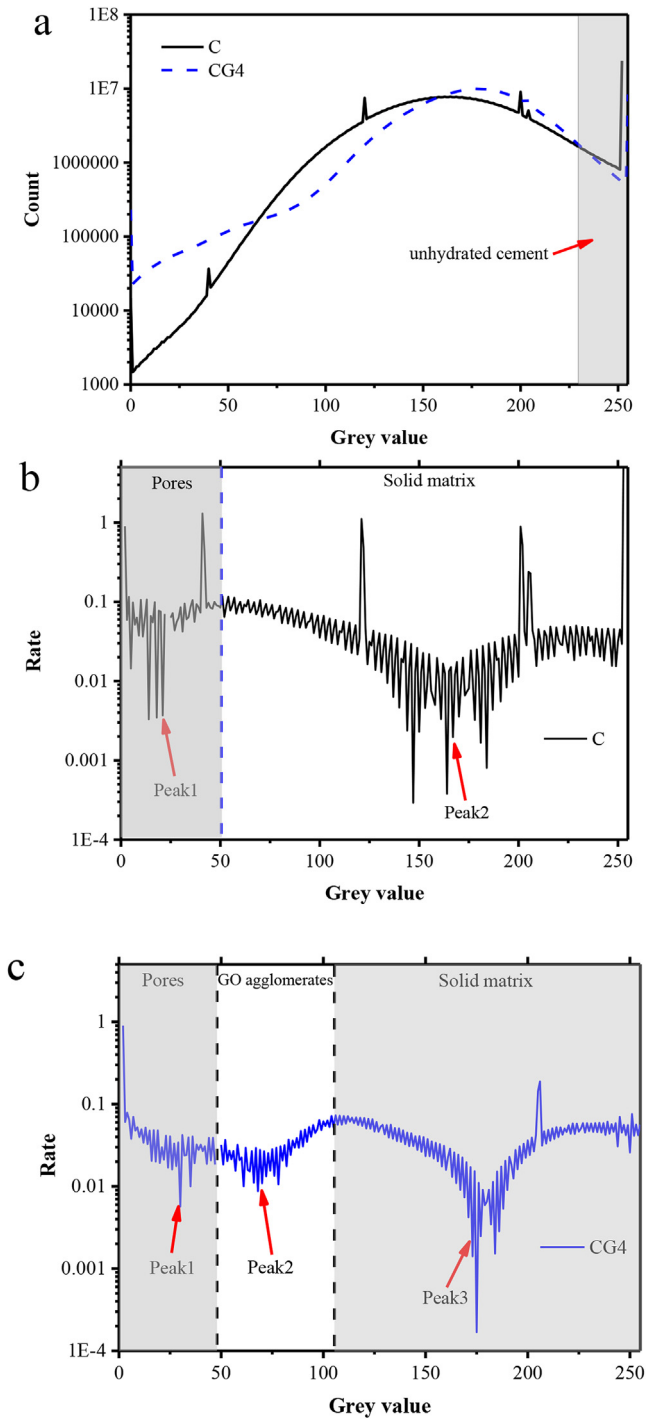

Fig. 5. (A) Gray value distribution of C and CG4; differential gray value distributions of C (b) and CG4 (c).

layer) GO cross-linked by calcium cations in saturated $Ca(OH)_2$ solution. Therefore, in Ref. [16], the GO absorbed on the cement surface was actually GO agglomerates formed in calcium-abundant solution.

Fig. 9 shows the deconvoluted Ca2p XPS spectra of samples C and CG4. By conducting peak fitting, it was shown that sample C contains CaO, $CaCO_3$, and $Ca(OH)_2$. However, sample CG4 contains not only CaO, $CaCO_3$, and $Ca(OH)_2$ but also $Ca(HCOO)_2$. It is believed that $Ca(HCOO)_2$ is formed by chelation between negatively charged carboxyl groups (–COOH) on the edge of GO nanosheets and calcium cations through ionic bonding [7]. Similar results were reported in Ref. [26]. Fig. 10 shows the deconvoluted C1s XPS spectra of samples C and CG4. By conducting peak fitting and deriving peak areas, it was found that CG4 contains a larger amount of sp^2 carbon (C=C) than that of sample C. For CG4, the ratio of sp^2 carbon to whole carbon content was 4%, whereas the value for sample C was 2%. This difference is reasonable because GO incorporation introduces a large amount of sp^2 carbon.

4.4. Electrical resistivity of cement paste incorporating GO

As shown in Fig. 11, it is evident that incorporation of GO increased the resistivity of the cement paste at 28 days. The resistivity of the cement paste first increased with the increase of GO content and reached a maximum when the GO content was 0.02%. The resistivity then decreased when the GO content further increased to 0.04%. However, it should be noted that CG2 and CG4 had almost identical resistivity values.

In a recent study [27], by using a noncontact electrical resistivity device, the effects of GO on early age (24 h) hydration was investigated by monitoring the resistivity development of cement paste incorporating GO. It was found that, with increasing GO content, the resistivity increased to a maximum when the GO content was 0.02% then decreased with further increasing of GO content. In this study, the general trend of resistivity development of cement paste with different amounts of GO is similar with what was reported by Li et al. [27]. However, the decrease of resistivity from CG2 to CG4 is not noticeable. That CG2 and CG4 have similar resistivity might be due to the GO dosage (0.02% by weight of cement) already being larger than the percolation threshold owing to the platelet-like morphology with very large aspect ratio of GO agglomerates [10].

The resistivity of cementitious composites has long been studied to investigate properties including cement hydration [28], microstructure [29], and durability [30]. The resistivity of the composite is related to the resistivity of each component, in addition to the proportions and distributions of the components. For cement paste incorporating GO, the following two components can be considered: 1). The solid matrix consisting of cement hydrates, unhydrated cement particles, and pores and 2). The dispersed GO agglomerates. Theoretically, one can estimate the resistivity of a composite by calculating the upper and lower limits of resistivity using parallel and series models. Before doing this, the resistivity and volume ratio of each component need to be known. As a result of oxidation, GO is an insulating material. However, there has been very limited information in the literature regarding the electrical resistivity of GO nanosheets. In this study, we used a simple test to estimate the resistivity of GO nanosheets rather than GO agglomerates. The resistivity of GO aqueous solutions with exactly known GO concentrations was measured. The solutions were contained in an acrylic container with inner dimension of 110 mm × 15 mm × 15 mm. Two copper plates, 15 mm × 15 mm × 3 mm, were glued at both ends of the container to serve as electrodes. The concrete resistivity meter (Giatec RCON™) was used to measure the resistivity of GO aqueous solutions. Before the resistivity test, mild sonication was performed on each GO solution to achieve good dispersion. The density of GO sheets was around 1.32 g/cm^3 [31]. Fig. 12 shows the resistivity development of GO solutions with increasing concentration. An initial guess for the resistivity of GO nanosheets had to be given to obtain the upper (parallel model) and lower (series model) limits until the measured resistivity was in the range of upper and lower limits. By doing so, the estimated resistivity of GO nanosheets was found to be ~0.003 Ω m, which is much lower than that of cement paste. It was also found that the concentration threshold for resistivity of the GO solution is ~0.003%, as shown in Fig. 12. Therefore, if GO nanosheets rather than GO agglomerates were dispersed within the cement paste, upper and lower limits for resistivity of the cement paste incorporating GO can be obtained.

The parallel model for resistivity of cement paste incorporating GO can be written as

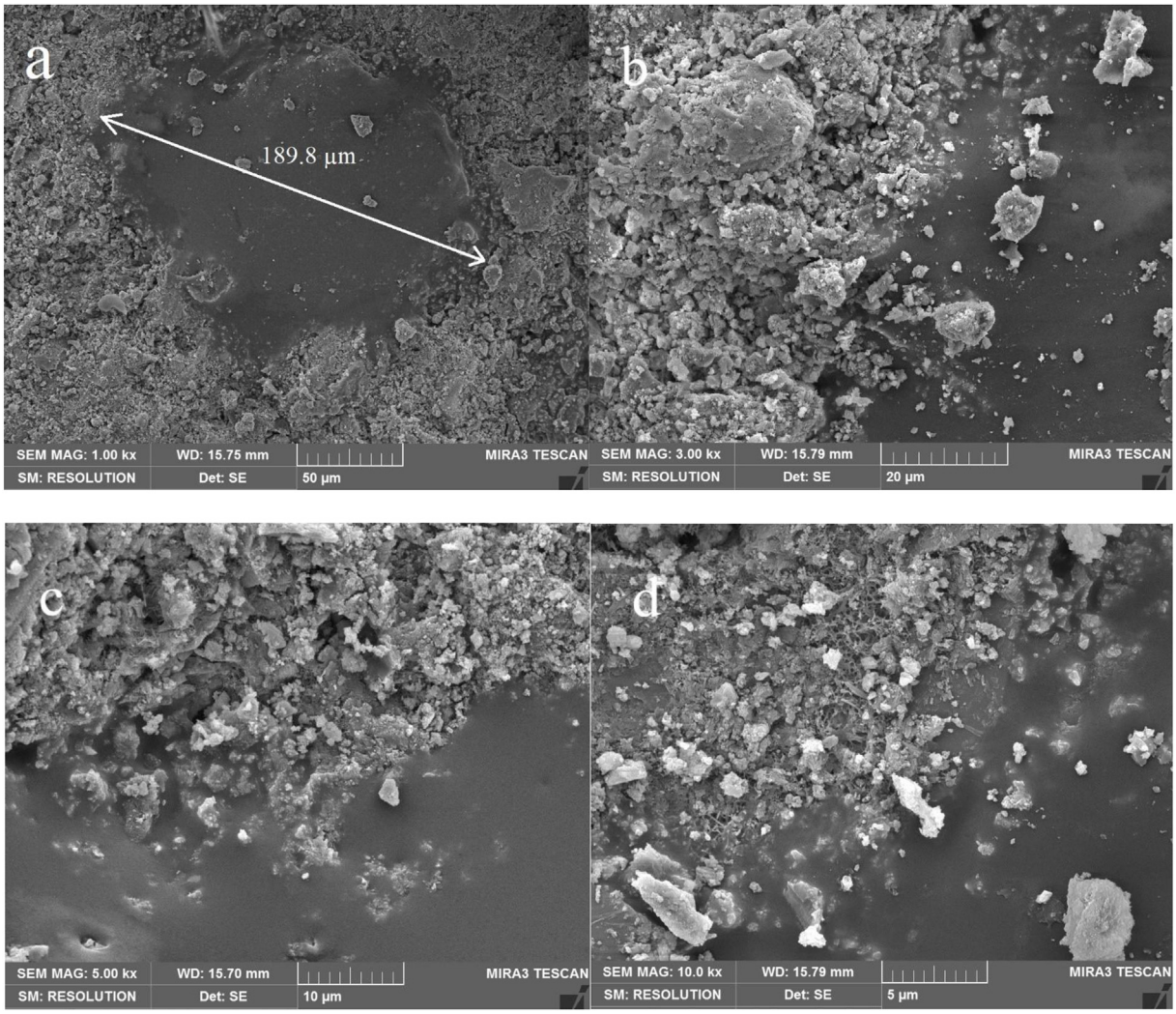

Fig. 6. SEM images of GO agglomerate.

$$\frac{1}{\rho_{series}} = \frac{1}{\rho_c} v_c + \frac{1}{\rho_{GO}} v_{GO}. \quad (3)$$

The series model for resistivity of cement paste incorporating GO can be written as

$$\rho_{parallel} = \rho_c v_c + \rho_{GO} v_{GO}, \quad (4)$$

where ρ_c and ρ_{GO} are the resistivity of cement paste and GO, respectively, and v_c and v_{GO} are the volume fractions of the cement matrix and GO, respectively.

As shown in Fig. 11, the measured resistivity of cement pastes with GO was not in the range of upper and lower limits. According to a previous study by the authors, the porosities of CG2 and CG4, 20.31% and 20.27%, were slightly reduced compared to that of C (20.48%). Therefore, the resistivities of the cement matrix of CG2 and CG4 should be quite close to that of cement matrix of C. Consequently, the effective resistivity of the cement paste is solely governed by the resistivity of GO dispersed in the cement matrix. If GO is well dispersed in the form of nanosheets, the effective resistivity of cement paste with GO will be in the range of upper and lower limits. However, the measured resistivity of cement pastes was much higher than the upper limits. Therefore, the analysis above shows that the GO in cement paste is not in the form of nanosheets. In addition, it is reasonable to conclude that the GO agglomerates are more electrically insulative than the cement matrix.

It was reported that the addition of well-dispersed carbon nanotubes and carbon nanofibers decreased the electrical resistivity of cement pastes effectively [19], which endows them with a self-sensing function. According to the current study, because the GO agglomerates are insulating, it is not possible to develop self-sensing cement-based materials if GO cannot be well dispersed in nanosheet form.

4.5. Effects of GO on flexural strength of cement paste

Fig. 13 shows the effects of GO on the flexural strength of cement paste at different GO dosages. It can be seen that the flexural strength was increased with an increase of GO dosage. Compared to control sample C, the flexural strengths of CG2 and CG4 were increased by 35% and 83%, respectively.

In previous studies [9,10], the authors investigated the effects of GO agglomerates, rather than GO nanosheets, on the properties of cement paste. It was found that GO agglomerates accelerate hydration, refine pore structure, and improve compressive and tensile splitting strength. According to mercury intrusion porosimetry (MIP) results [9], the porosities of CG2 and CG4, 20.31% and 20.27%, were slightly reduced compared to that of C (20.48%). Therefore, it is reasonable to assume that the improvement of flexural strength was mainly due to reinforcing effect of GO agglomerates. According to previous studies, GO agglomerates have high aspect ratio [10], strong interlayer shear stress, and strong tensile strength [7]. In this study, it was further proved that GO agglomerates have slender platelet-like shape and good bonding with the cement matrix.

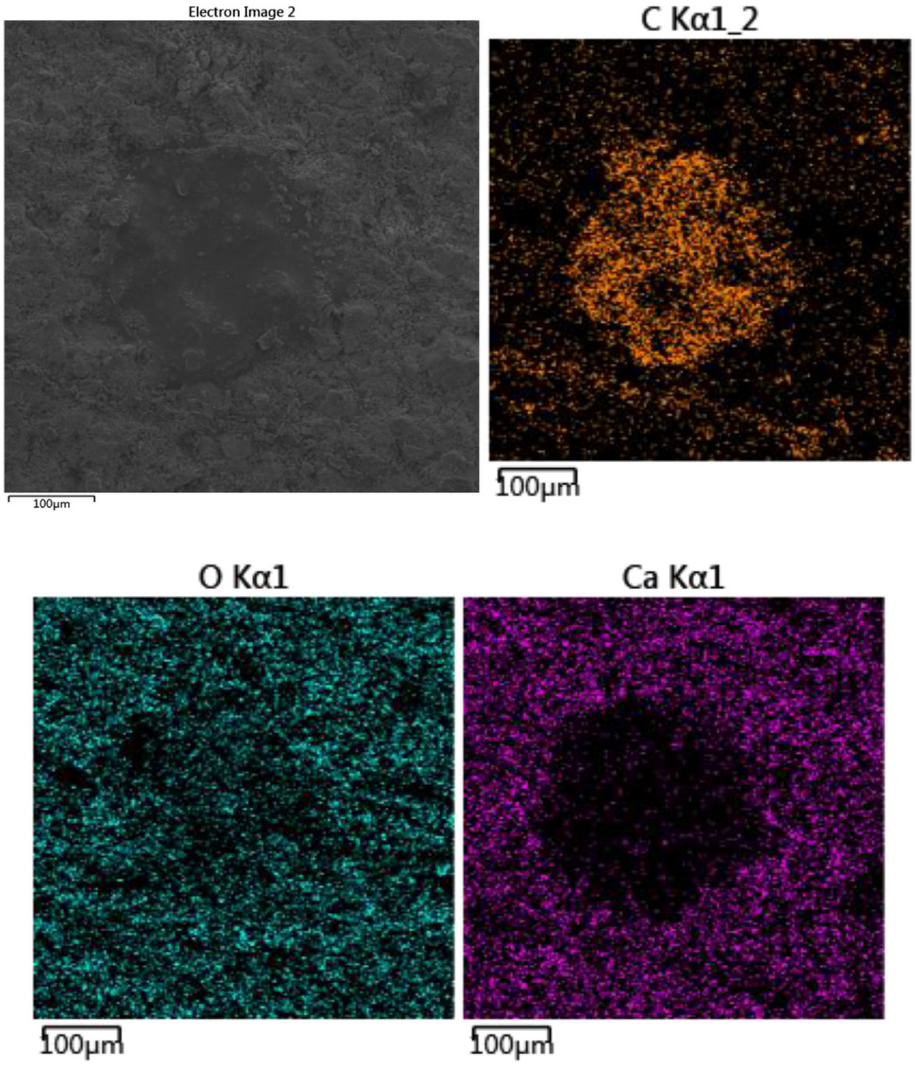

Fig. 7. EDS analysis of GO agglomerate.

For composites reinforced with fillers, the reinforcing effect of filler can be quantified by increase of the Young's modulus. By applying rule of mixtures, the Young's modulus (stiffness) of composites, E_m, can be estimated as [32]:

$$E_{comp} = \eta_l \eta_o E_{filler} V_{filler} + E_m(1 - V_{filler}) \tag{5}$$

where E_{filler}, E_m denote the Young's modulus of the filler and matrix, respectively. V_{filler} and V_m correspond to the volume fraction of the filler and matrix. Length efficiency factor η_l and Krenchel orientation factor η_o are included to correct deviations. The length efficiency factor η_l of the fillers in the nanocomposites can be defined as [32]:

$$\eta_l = 1 - \frac{\tanh(ns/2)}{ns/2} \tag{6}$$

$$n = \sqrt{\frac{2G_m}{E_{filler}}\left(\frac{V_{filler}}{1 - V_{filler}}\right)} \tag{7}$$

where G_m is shear modulus of matrix, the filler aspect ratio s is defined as the ratio of length and thickness for platelet. The length efficiency factor, which vary between 0 and 1, quantifies the effect of aspect ratio

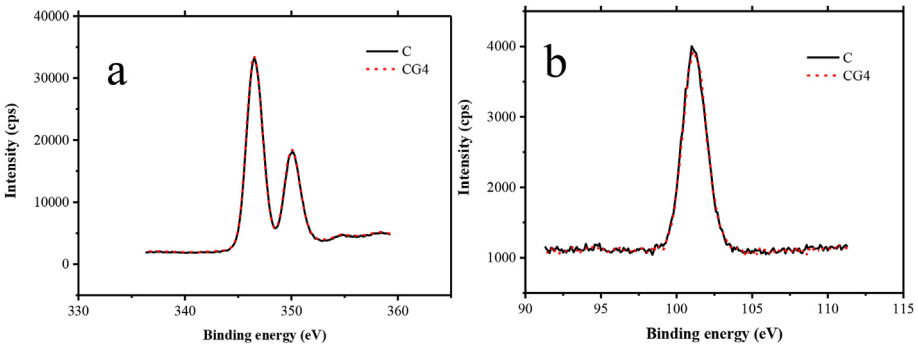

Fig. 8. Ca2p (a) and Si2p (b) XPS spectra of C and CG4.

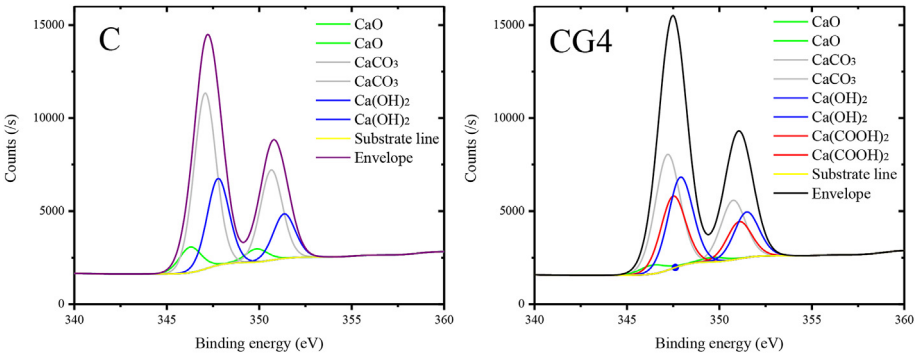

Fig. 9. Deconvoluted Ca2p XPS spectra of C and CG4.

of the filler on the mechanical properties of the composites. In addition to aspect ratio of filler, efficient stress transfer between matrix and filler is also important for reinforcing effect. The axial stress taken by the filler can be estimated by Ref. [32]:

$$\sigma_{filler} = E_{filler}\varepsilon_m\eta_l \quad (8)$$

where ε_m is strain of the matrix. According to Eqs. (5)–(8), high aspect ratio is preferred for improving mechanical properties of the composites. Therefore, based on above discussions, the improvement in flexural strength could be ascribed to the special 2D morphology of GO agglomerates, especially its high aspect ratio. This is consistent with the results reported by May et al. [33], in which they showed a sharp increase in reinforcing efficiency as the aspect ratio is increased from 1000 to 2000 b < superscript > < /superscript > y conducting both experimental and theoretical analysis. In addition to large aspect ratio, crack deflection [21] effect of GO agglomerates and improved mechanical interlocking [21] at the GO agglomerates-matrix interface may also contribute to the strength improvement.

5. Conclusions

In this study, by using X-ray μCT, it was proved that GO agglomerates with lateral size up to hundreds of micrometers formed in the cement paste if no dispersion agent was applied. Meanwhile, little GO was found to be absorbed onto surfaces of cement particles and hydration products. By measuring electrical resistivity, the GO agglomerates were found to be electrically more insulative than cement paste. However, GO agglomerates reinforce the flexural strength of the cement paste because of their special morphology and intrinsic strength. From a dispersion perspective, for GO-reinforced cement composites, one option is to incorporate multilayer GO, which reduces the production cost of GO and facilitates dispersion; another option is to develop a dispersion agent specially designed for GO that can disperse single-sheet GO uniformly in cement composites.

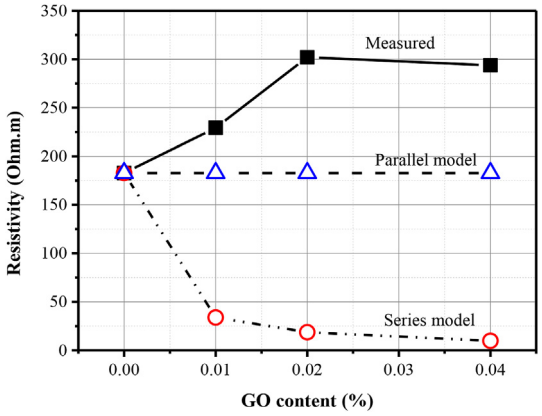

Fig. 11. Electrical resistivity of cement paste incorporating GO.

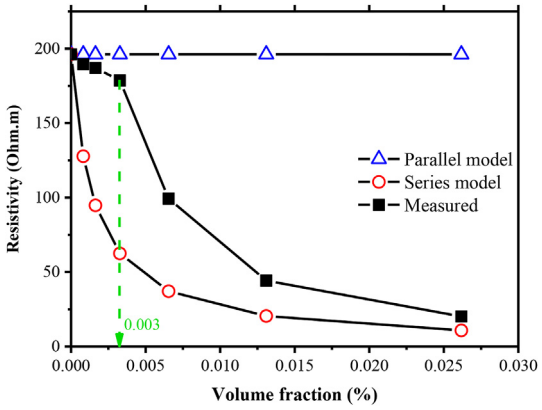

Fig. 12. Electrical resistivity development of GO aqueous solutions.

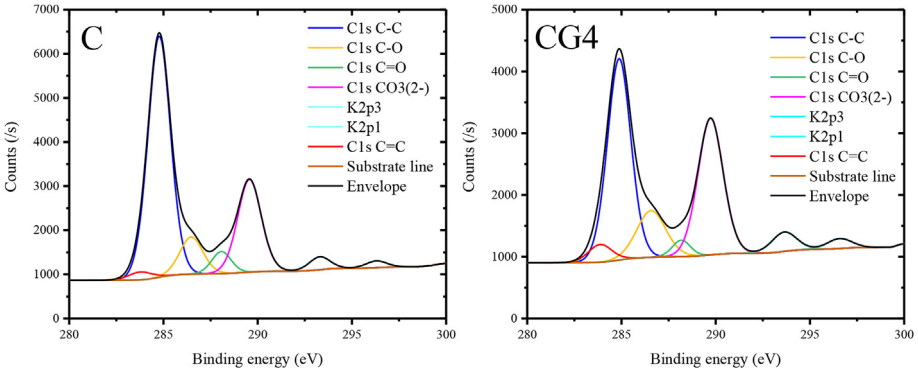

Fig. 10. Deconvoluted C1s XPS spectra of C and CG4.

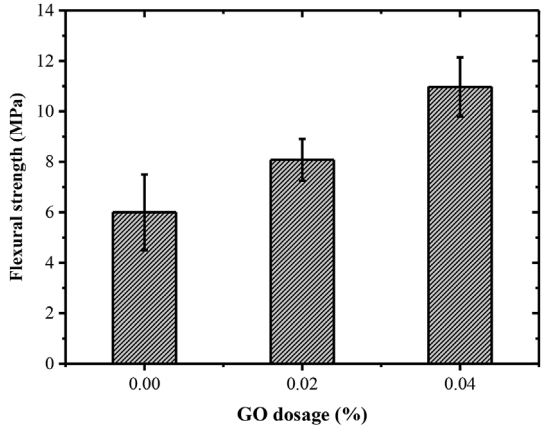

Fig. 13. Flexural strength of cement paste samples C, CG2, and CG4.

Acknowledgment

Xiangyu Li is grateful for the financial support of the Hundred Young Talents Plan of Shanxi province (02010016) in conducting this study. Wen Hui Duan is grateful for the financial support of the Australian Research Council (IH150100006) in conducting this study.

Appendix A. Supplementary data

Supplementary data related to this article can be found at http://dx.doi.org/10.1016/j.cemconcomp.2018.06.008.

References

[1] A.M. Dimiev, T.A. Polson, Contesting the two-component structural model of graphene oxide and reexamining the chemistry of graphene oxide in basic media, Carbon 93 (2015) 544–554.
[2] H. Yang, H. Cui, W. Tang, Z. Li, N. Han, F. Xing, A critical review on research progress of graphene/cement based composites, Composites Part a 102 (2017) 273–296.
[3] Z. Lu, D. Hou, L. Meng, G. Sun, C. Lu, Z. Li, Mechanism of cement paste reinforced by graphene oxide/carbon nanotubes composites with enhanced mechanical properties, RSC Adv. 5 (122) (2015) 100598–100605.
[4] Z. Lu, A. Hanif, G. Sun, R. Liang, P. Parthasarathy, Z. Li, Highly dispersed graphene oxide electrodeposited carbon fiber reinforced cement-based materials with enhanced mechanical properties, Cement Concr. Compos. 87 (2018) 220–228.
[5] X. Li, C. Li, Y. Liu, S.J. Chen, C.M. Wang, J.G. Sanjayan, W.H. Duan, Improvement of mechanical properties by incorporating graphene oxide into cement mortar, Mech. Adv. Mater. Struct. (2017), http://dx.doi.org/10.1080/15376494.2016.1218226.
[6] D. Hou, Z. Lu, X. Li, H. Ma, Z. Li, Reactive molecular dynamics and experimental study of graphene-cement composites: Structure, Dynamics and Reinforcement Mechanisms. Carbon 115 (2017) 188–208.
[7] S. Park, K.-S. Lee, G. Bozoklu, W. Cai, S.T. Nguyen, R.S. Ruoff, Graphene oxide papers modified by divalent ions—enhancing mechanical properties via chemical cross-linking, ACS Nano 2 (3) (2008) 572–578.
[8] X. Li, A.H. Korayem, C. Li, Y. Liu, H. He, J.G. Sanjayan, W.H. Duan, Incorporation of graphene oxide and silica fume into cement paste: a study of dispersion and compressive strength, Construct. Build. Mater. 123 (2016) 327–335.
[9] X. Li, Y.M. Liu, W.G. Li, C.Y. Li, J.G. Sanjayan, W.H. Duan, Z. Li, Effects of graphene oxide agglomerates on workability, hydration, microstructure and compressive strength of cement paste, Construct. Build. Mater. 145 (2017) 402–410.
[10] X. Li, Z. Lu, S. Chuah, W. Li, Y. Liu, W.H. Duan, Z. Li, Effects of graphene oxide aggregates on hydration degree, sorptivity, and tensile splitting strength of cement paste, Compos. Appl. Sci. Manuf. 100 (2017) 1–8.
[11] Z. Lu, X. Li, A. Hanif, B. Chen, P. Parthasarathy, J. Yu, Z. Li, Early-age interaction mechanism between the graphene oxide and cement hydrates, Construct. Build. Mater. 152 (2017) 232–239.
[12] Z. Lu, A. Hanif, C. Ning, H. Shao, R. Yin, Z. Li, Steric stabilization of graphene oxide in alkaline cementitious solutions: mechanical enhancement of cement composite, Mater. Des. 127 (2017) 154–161.
[13] Z. Wang, J. Gao, T. Ai, W. Jiang, P. Zhao, Quantitative evaluation of carbon fiber dispersion in cement based composites, Construct. Build. Mater. 68 (2014) 26–30.
[14] J. Gao, Z. Wang, T. Zhang, L. Zhou, Dispersion of carbon fibers in cement-based composites with different mixing methods, Construct. Build. Mater. 134 (2017) 220–227.
[15] M. Murugan, M. Santhanam, S. Sen Gupta, T. Pradeep, S.P. Shah, Influence of 2D rGO nanosheets on the properties of OPC paste, Cement Concr. Compos. 70 (2016) 48–59.
[16] M. Wang, R. Wang, H. Yao, Z. Wang, S. Zheng, Adsorption characteristics of graphene oxide nanosheets on cement, RSC Adv. 6 (68) (2016) 63365–63372.
[17] N.S. Andryushina, O.L. Stroyuk, I.B. Yanchuk, A.V. Yefanov, A dynamic light scattering study of photochemically reduced colloidal graphene oxide, Colloid Polym. Sci. 292 (2) (2014) 539–546.
[18] J.F. Moulder, J. Chastain, Handbook of X-ray Photoelectron Spectroscopy a Reference Book of Standard Spectra for Identification and Interpretation of XPS Data, Physical Electronics Division, Perkin-Elmer Corp, Eden Prairie, Minn.: Eden Prairie, Minn., 1992.
[19] M.S. Konsta-Gdoutos, C.A. Aza, Self sensing carbon nanotube (CNT) and nanofiber (CNF) cementitious composites for real time damage assessment in smart structures, Cement Concr. Compos. 53 (2014) 162–169.
[20] J. Zhang, Z. Li, Application of GEM Equation in microstructure Characterization of cement-based materials, J. Mater. Civ. Eng. 21 (11) (2009) 648–656.
[21] M.A. Rafiee, J. Rafiee, Z. Wang, H. Song, Z.-Z. Yu, N. Koratkar, Enhanced mechanical properties of nanocomposites at low graphene content, ACS Nano 3 (12) (2009) 3884–3890.
[22] C.D. Williams, P. Carbone, F.R. Siperstein, Computational characterisation of dried and hydrated graphene oxide membranes, Nanoscale 10 (4) (2018) 1946–1956.
[23] S. Kim, J. Lee, S.-S. Lee, Fractionation of graphene oxides by size-selective adhesion with spherical particles, Macromol. Res. 24 (12) (2016) 1098–1104.
[24] X. Kong, S. Emmerling, J. Pakusch, M. Rueckel, J. Nieberle, Retardation effect of styrene-acrylate copolymer latexes on cement hydration, Cement Concr. Res. 75 (2015) 23–41.
[25] D.R. Dreyer, S. Park, C.W. Bielawski, R.S. Ruoff, The chemistry of graphene oxide, Chem. Soc. Rev. 39 (1) (2010) 228–240.
[26] M. Wang, R. Wang, H. Yao, S. Farhan, S. Zheng, C. Du, Study on the three dimensional mechanism of graphene oxide nanosheets modified cement, Construct. Build. Mater. 126 (2016) 730–739.
[27] W. Li, X. Li, S.J. Chen, Y.M. Liu, W.H. Duan, S.P. Shah, Effects of graphene oxide on early-age hydration and electrical resistivity of Portland cement paste, Construct. Build. Mater. 136 (2017) 506–514.
[28] L. Xiao, Z. Li, Early-age hydration of fresh concrete monitored by non-contact electrical resistivity measurement, Cement Concr. Res. 38 (3) (2008) 312–319.
[29] Z. Liu, Y. Zhang, Q. Jiang, Continuous tracking of the relationship between resistivity and pore structure of cement pastes, Construct. Build. Mater. 53 (2014) 26–31.
[30] S.W. Tang, Y. Yao, C. Andrade, Z.J. Li, Recent durability studies on concrete structure, Cement Concr. Res. 78 (Part A) (2015) 143–154.
[31] X. Sun, D. Luo, J. Liu, D.G. Evans, Monodisperse chemically modified graphene obtained by density gradient ultracentrifugal rate separation, ACS Nano 4 (6) (2010) 3381–3389.
[32] Li, Z. Raman, Spectroscopic Studies of the Mechanics of Graphene-based Nanocomposites (PhD Thesis), The University of Manchester, 2015.
[33] P. May, U. Khan, A. O'Neill, J.N. Coleman, Approaching the theoretical limit for reinforcing polymers with graphene, J. Mater. Chem. 22 (4) (2012) 1278–1282.